High-Resolution Imaging of Fission Energy Neutrons

P. Marleau[1], M. A. Blackston[2], J. Brennan[1], E. Brubaker[1], M. Gerling[1], P. A. Hausladen[2], K. McMillan[1], S. Mrowka[1], and J. Newby[2]

[1] *Sandia National Laboratories, Livermore, CA 94550 USA*[*]

[2] *Oak Ridge National Laboratory, Oak Ridge, TN, 37831 USA*

ABSTRACT

Because of their penetrating power, energetic neutrons and gamma rays (~1 MeV) offer the best possibility of detecting, localizing, and characterizing special nuclear material (SNM). There is a class of applications, including arms control and treaty verification, in which high resolution fast neutron imaging can help determine the absence, presence, and/or distribution of SNM. In this paper we will present the development of high-resolution fast neutron imagers capable of not only detecting, but characterizing the spatial distribution of SNM. Results from laboratory tests of several fast neutron imagers with extended neutron source distributions are discussed.

INTRODUCTION

High resolution fast neutron imaging is a potentially useful tool for applications that require the verification of the absence, presence, and/or distribution of special nuclear material (SNM). In such applications, the ability to distinguish an extended source from a point source is often valuable. Additionally, resolving multiple extended sources is more difficult than similarly situated point sources. Here we present several fast neutron imaging concepts and their performance in laboratory tests with extended neutron source distributions.

In researching various fast neutron imaging concepts, we find that detection efficiency and angular resolution are often opposing constraints. These parameters must be balance and optimized for a particular application. Understanding how these constraints drive detector design at both ends of the spectrum is critical in determining the ultimate capabilities of different imaging technologies.

NEUTRON SCATTER CAMERA

The Neutron Scatter Camera (NSC), shown in Figure 1, consists of 32 EJ-309 (1) liquid scintillator cells arranged in two planar arrays of 16 cells each. Each cylindrical cell is optically coupled to a single photomultiplier tube (PMT). Neutron scatter camera designs have been described previously (2) (3) (4) (5).

[*] Sandia National Laboratories is a multi-program laboratory managed and operated by Sandia Corporation, a wholly owned subsidiary of Lockheed Martin Corporation, for the U.S. Department of Energy's National Nuclear Security Administration under Contract DE-AC04-94AL85000. SAND Number 2012-.

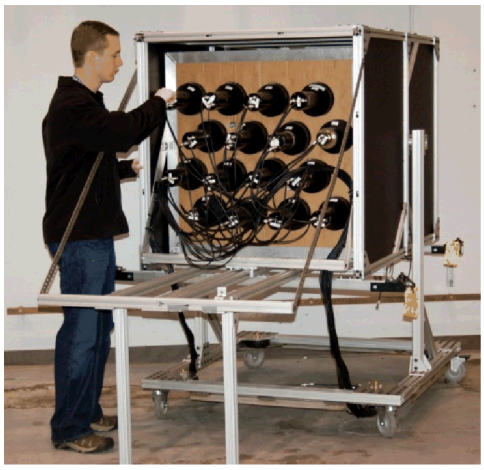

Figure 1: Photograph of the 32-element Neutron Scatter Camera

To investigate the scatter camera's imaging performance for extended sources, a 50 cm diagonal line source was simulated by integrating over an extended period of time as a Cf252 point source was moved.

Figure 2 shows one of the results of the application of a Maximum Likelihood Estimator Maximizer (MLEM) imaging reconstruction technique (6) on a 96 hour data set with the line source at a 3 meter stand-off. It was found that large integration times were required as the NSC is designed/optimized for enhancing signal to background in low-signal situations, not for high resolution imaging.

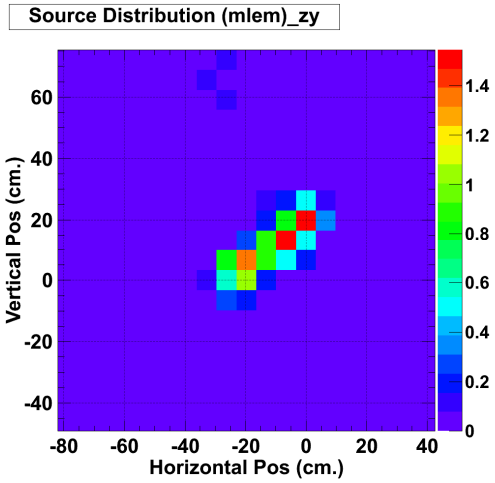

Figure 2: MLEM reconstructed image from the NSC of a 50 cm. long diagonal neutron source with a 96 hour dwell time.

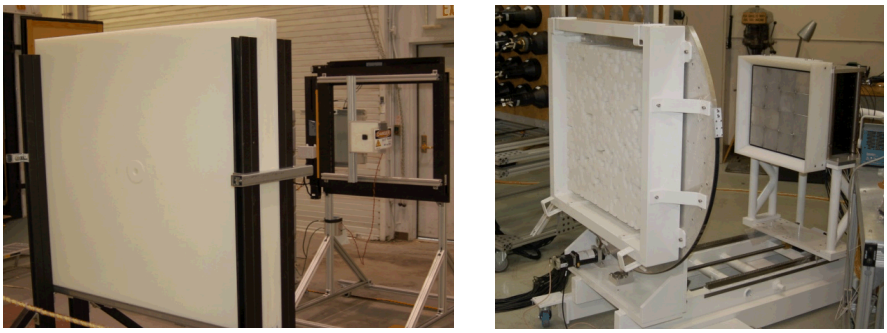

Figure 3: (Left) Photograph of a pinhole fast neutron imager. (Right) Photograph of a coded aperture fast neutron imager.

CODED APERTURE IMAGERS

An alternative imaging technique explored is based on coded aperture imaging (7) (8) (9). Both single aperture (pinhole) and coded aperture mask patterns were explored (Figure 3). In both cases 10 centimeters of high density polyethylene (HDPE) was used to modulate the fast neutrons. Imaging is achieved by de-convolving the projected aperture pattern using a calculated detector response matrix.

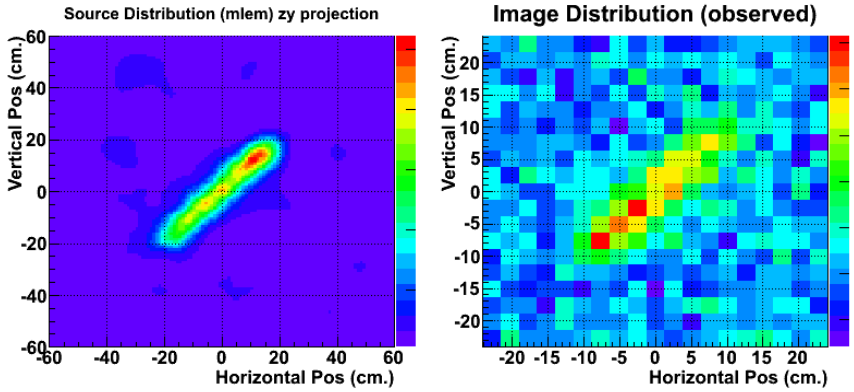

Figure 4: (Right) Raw neutron distribution on the image plane of the pinhole imager. (Left) MLEM reconstructed image.

In the case of the pinhole imager, the response matrix is simply the point spread function of the aperture. Figure 4 shows images from the pinhole aperture imager with the same 50 cm. diagonal neutron line source with an equivalent dwell time of 18 minutes indicating that aperture imaging may be better suited to high resolution imaging than the NSC.

A series of measurements were also conducted using extended source distributions at Sandia National Labs. Both the NSC and the coded aperture imager shown in Figure 3 (right) developed in a collaboration between Sandia National Laboratories and Oak Ridge National Laboratory were used (10) (11). Three different aperture patterns were used for these measurements; two tiled 19x19 Uniformly Redundant Arrays (URA) (1.4 and 2.0 cm elements) and an optimized random aperture (2.0 cm elements).

An important design characteristic of a coded aperture imager that determines the expected signal to noise of an extended source distribution is the open fraction of its

mask. There have been several approaches to calculating the optimum open fraction of a mask array (12) (13). By employing a heuristic optimization routine on a collection of randomly selected mask patterns we were able to produce aperture patterns with any open fraction ranging from a pinhole aperture to an inverse pinhole aperture that provide the maximum signal to noise for a given source distribution.

The widely employed uniformly redundant array (URA) mask exists only for a certain number of open fractions. In fact there are very few known URAs with open fraction significantly different from 50%. In the past, motivation for using the URA mask stemmed from the fact that matched filtering could be employed to allow for the source distribution to be reconstructed from the coded image by directly correlating the coded image with the aperture array itself. Because the URA autocorrelation function has constant side-lobes, matched filtering was ideal because the reconstruction was not subject to certain systematic errors that other, non-URA, arrays like random masks would display if matched filtering was employed (14). With the advancement of iterative image reconstruction algorithms such as maximum likelihood expectation maximization (MLEM) (6) and computer systems to handle their computationally intense nature, the need for matched filtering techniques is diminished.

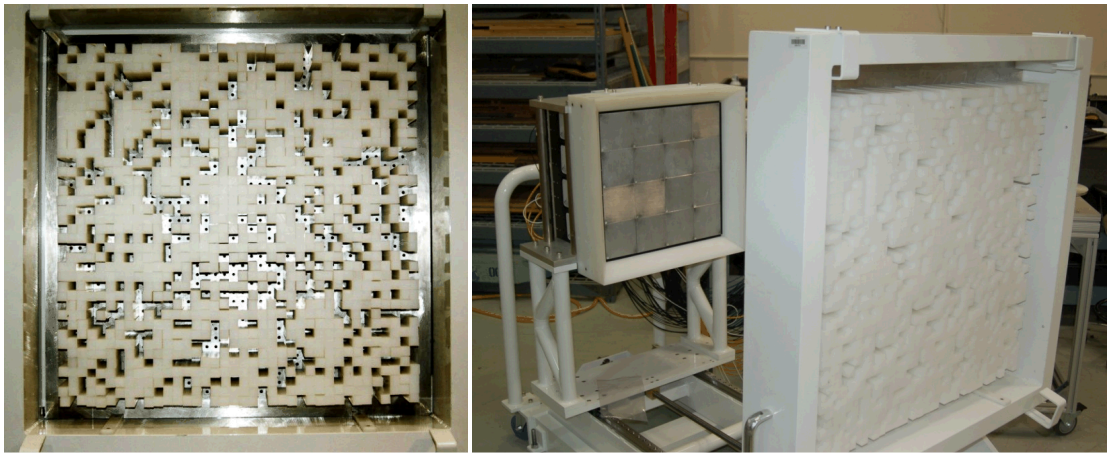

Figure 5: Photograph of the optimized mask used in the extended source measurement campaign (left) and coded aperture imager with mask installed (right).

The mask shown in Figure 5, optimized for a source distribution similar to that seen in Figure 6 has an open fraction of ~30%. The mask was optimized in an iterative algorithm by flipping a random subset of mask elements and comparing the reconstructed image of a simulated data set to the true source distribution by a chi-squared. The sum of chi-squared values for 50 simulated trials was compared to a threshold value. If the mask's performance passed the threshold, then it was kept for the next iteration and the threshold value lowered. Otherwise, the mask was rejected and the number of mask elements flipped was reduced by one.

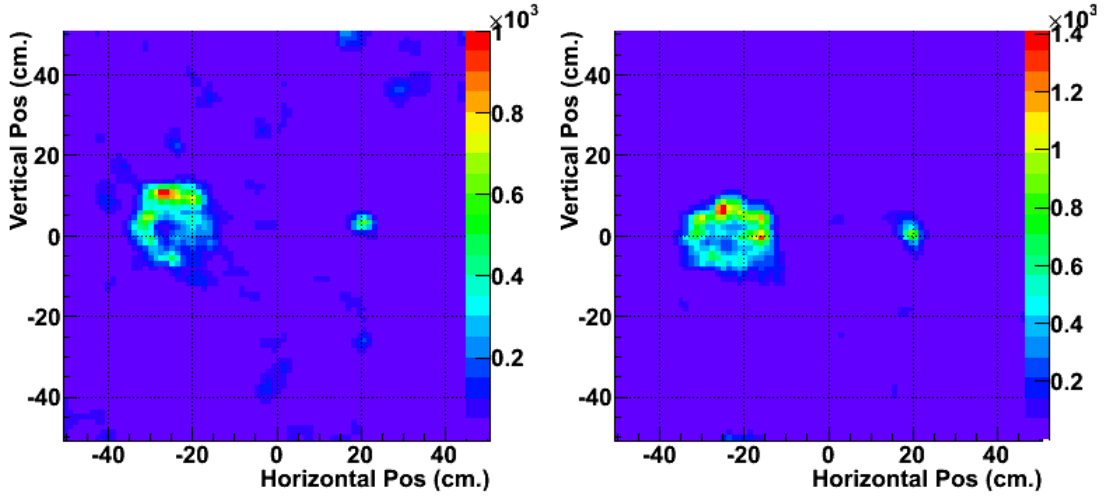

Figure 6: MLEM reconstructed images of an extended source plus point source after 1 hour of dwell time for the 19x19 URA (2cm aperture) (left) and optimized mask (2cm aperture) (right).

Many extended and point source configurations were explored. Figure 6 shows the MLEM reconstructed images (200 iterations) of an extended plus point source after 1 hour of dwell time. In all cases a ^{252}Cf (~4x10^5 n/s) was used to construct the extended source by moving it through a 3 dimensional pattern during the measurement period. A bin by bin comparison between these two images to the expected true source distribution indicates that the optimized mask is indeed the better performer.

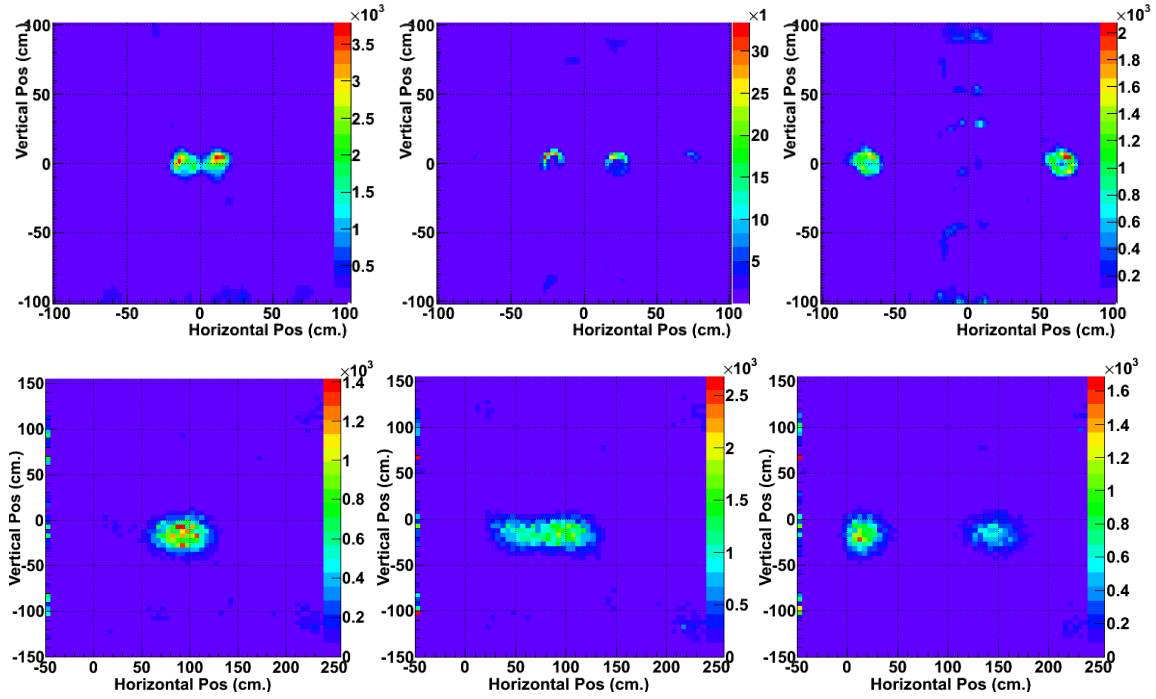

Figure 7: MLEM reconstructed images of two extended sources at various separation distances for the 19x19 URA coded aperture imager (1 hour dwell time) (top row) and Neutron Scatter Camera (bottom row) (3 days dwell (left), 3 days dwell (center), 1.25 days dwell (right)).

Figure 7shows a comparison between the 19x19 URA coded aperture imager and the NSC. As can be seen, the coded aperture imager is better suited to high resolution imaging of extended sources. Higher resolution images are apparent in much shorter dwell times. This is in part due to the higher intrinsic resolution of the coded aperture imager and in part due to the low neutron detection efficiency of the NSC. Because NSC imaging relies on reconstructing the kinematics of two interactions within the detector, its imaging efficiency is further reduced by its efficiency to detect the second interaction.

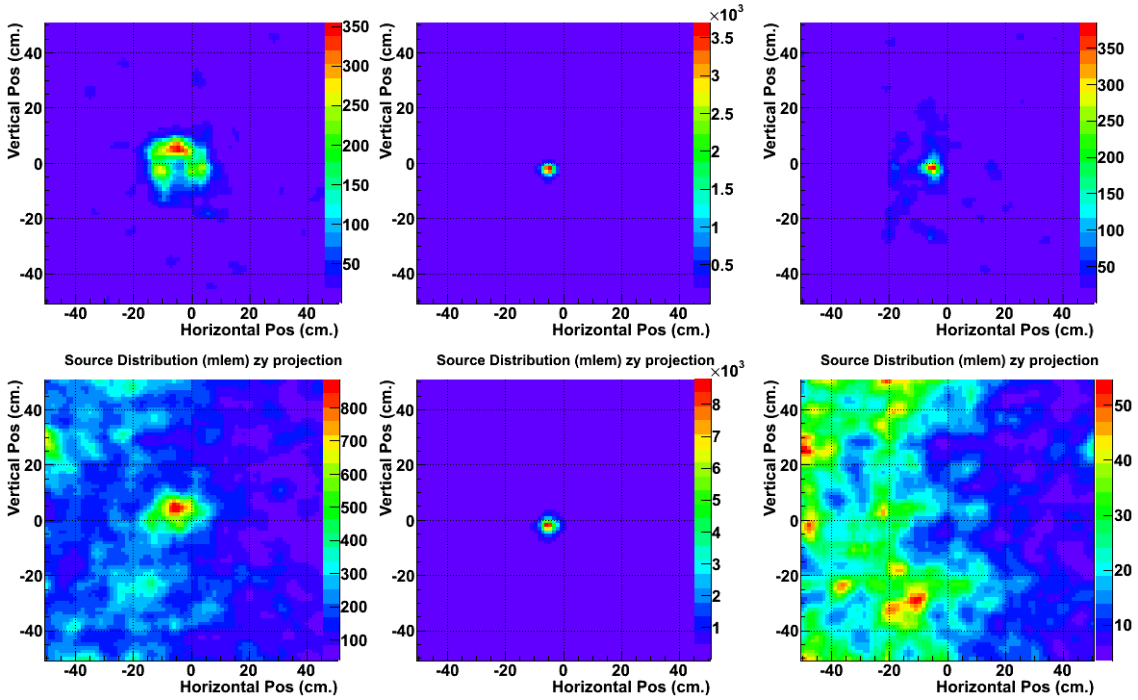

Figure 8: MLEM reconstructed images of an extended source through 4" HDPE shielding (left column), point source through 4" HDPE shielding (center column), and point source through 4" HDPE + 4" lead shielding (right column) using detected neutrons (top row) and gamma-rays (bottom row) from the 19x19 URA coded aperture imager (1 hour dwell).

Finally, because the coded aperture imager utilizes liquid organic scintillator as its detection material, neutron events can be discriminated by gamma events by the shape of the time distribution of scintillation light. This allows for the possibility to image simultaneously in neutron as well as gamma-rays. Though the HDPE mask is not the optimum material for attenuating gammas, it does modulate well enough to produce images such as in Figure 8 (bottom).

Figure 8 compares the reconstructed neutron images (top row) to the gamma images (bottom row) for a single extended source through four inches of HDPE (left column), a single point source through four inches of HDPE (center column), and a single point source through four inches of HDPE plus four inches of lead (right column). It can be seen that the coded aperture imager can easily distinguish between extended and point sources in both neutrons and gamma-rays even through significant low-Z shielding. However, when presented with significant low and high-Z shielding only the neutrons

have sufficient penetrating power to be detected and imaged. The gamma-ray rates and image in Figure 8 (bottom right) are consistent with background.

CONCLUSIONS

We have shown that coded aperture imaging is well suited to applications in which the absence, presence, and/or distribution of SNM is to be characterized or verified. High resolution neutron images can be obtained even through significant shielding in reasonable dwell times, a feat that is not easily accomplished through other neutron imaging techniques. Because of their penetrating power, neutron imaging offers the possibility of characterizing the distribution of SNM even through significant low and high-Z shielding materials where gamma-ray detection and imaging are likely to fail.

ACKNOWLEDGEMENTS

This work was supported by NA-221, the Office of Non-Proliferation R&D of the NNSA.
Sandia National Laboratories is a multi-program laboratory managed and operated by Sandia Corporation, a wholly owned subsidiary of Lockheed Martin Corporation, for the U.S. Department of Energy's National Nuclear Security Administration under Contract DE-AC04-94AL85000. SAND Number 2012-

REFERENCES

1. **Eljen.** EJ-309 data sheet. [Online] http://www.eljentechnology.com/datasheets/EJ309%20data%20sheet.pdf.
2. *Advances in Imaging Fission Neutrons with a Neutron Scatter Camera.* **Marleau, P., et al.** Honolulu, HI : IEEE NSS-MIC, 2007.
3. *Calibration of the Fast Neutron Imaging Telescope (FNIT) Prototype Detector.* **Bravar, Ulisse, Richard S. Woolf, Paul J. Bruillard, Erwin O. Fluckiger, Jason S. Legere, Alec L. MacKinnon, John R. Macri, et al.** IEEE Transactions on Nuclear Science, Vol. 56.
4. *A large double scatter telescope for gamma rays and neutrons.* **D. Herzo, R. Koga, W.A. Millard, S. Moon, J. Ryan, R. Wilson, A.D. Zych, R.S. White.** 3, February 1, 1975, Nuclear Instruments and Methods A, Vol. 123, pp. 583-597. ISSN 0029-554X.
5. *Design of a Large-Area Fast Neutron Directional Detector.* **Vanier, P.E., et al., et al.** 2006. Nuclear Science Symposium Conference Record. Vol. 1, pp. 93-97.
6. *Maximum likelihood reconstruction for emission tomography.* **Shepp, L A, and Y Vardi.** 2, 1982, IEEE transactions on medical imaging, Vol. 1, pp. 113-122.
7. *Coded Aperture Imaging in X- and Gamma-Ray Astronomy.* **Caroli, E., et al.** 1987, Space Science Reviews, Vol. 45, pp. 349-403.
8. *Coded aperture imaging with uniformly redundant arrays.* **Fenimore, E. E., and T. M. Cannon.** 3, 1978, Applied Optics, Vol. 17.
9. *Results from the Coded Aperture Neutron Imaging System.* **Marleau, P., Brennan, J., Brubaker, E., Steele, J.** Knoxville : s.n., 2010. IEEE Nuclear Science Symposium.
10. **Hausladen, P. and Blackston, M.** *Passive and Active Fast-Neutron Imaging in Supoort of AFCI Safeguards Campaign.* s.l. : Oak Ridge National Laboratory, 2009. ORNL/TM-2009/210.

11. *FAST-NEUTRON CODED-APERTURE IMAGING FOR WARHEAD COUNTING.* **Brown, B. L., Marleau, P., Newby, J., Brubaker, E., Fabris, L., Blackston, M. A., Hausladen, P. A.** Desert Springs : s.n., 2011. INMM.
12. *Signal-to-noise ratio in coded aperture imaging.* **P.M.E. Shuttler, etal.** s.l. : Nuclear Instrumentation and Methods A, 2011. doi:10.1016/j.nima.2011.12.023.
13. *Coded Apertures: Past, Present, and Future Application and Design.* **Gottesman, S.R.** 2007. Proc. of SPIE. Vol. 6714.
14. *New family of binary arrays for coded aperture imaging.* **Gottesman, Stephen R., and E. E. Fenimore.** 20, 1989, Applied Optics , Vol. 28.
15. *Coded Aperture Optimization using Monte Carlo simulations.* **Martineau, etal.** 2010, Nculear Instrumentation and Methods A. doi:10.1016/j.nima.2010.02.261.